Ukrainian Journal of Physical Optics
ISSUE 4
2026

Thermal-Feedback-Induced Transmission Symmetry Breaking in an Asymmetric Microcavity

Min She*, Guohao Shi

School of Computer Engineering, Jiangsu University of Architectural Technology, Xuzhou 221116, China
*Corresponding author: m.she@smail.nju.edu.cn

Received: 15.07.2026

Abstract. Transmission symmetry breaking is important for realizing direction-selective light transport in integrated photonics, while existing approaches generally rely on magneto-optical materials, temporal modulation, or strong optical nonlinearities. We theoretically investigate thermal-feedback-induced transmission symmetry breaking in an asymmetric Fabry-Pérot microcavity filled with polydimethylsiloxane. Due to unequal mirror reflectivities, counterpropagating optical fields exhibit different coupling efficiencies and absorption powers, resulting in distinct thermally induced resonance shifts and transmission characteristics. Numerical results show that the proposed nonmagnetic structure can achieve a transmission contrast exceeding 50 dB. The proposed mechanism provides a simple approach for realizing compact integrated photonic devices with direction-selective transmission.

Keywords: thermo-optic nonlinearity, asymmetric Fabry-Pérot microcavity, transmission symmetry breaking, fiber-integrated
UDC: 535.3
DOI: 10.3116/16091833/Ukr.J.Phys.Opt.2026.04077

1. Introduction

As a core foundation of optical information processing systems, direction-selective optical transmission has wide application prospects in integrated photonics, optical communications, and optical sensing. Currently, most approaches are based on the magneto-optical effect [1-6]. However, these devices require magnetic materials and external magnetic fields to break time-reversal symmetry, leading to large size, complex fabrication, and difficult optical coupling. Therefore, developing magnetic-field-free, simply structured, and integrable schemes to break transmission symmetry is of vital importance.

In recent years, direction-dependent optical transmission has been widely explored through mechanisms such as spatiotemporal modulation [7-12], Doppler effects [13-15], optomechanical interactions [16-18], and optical nonlinearities [19-24]. Among them, approaches based on optical nonlinearities have attracted considerable attention due to their magnet-free operation and ease of integration. For example, integrating Kerr nonlinear materials with photonic platforms enables the miniaturization and integration of direction-selective photonic devices [25-27]. However, the inherently weak Kerr nonlinearity of most materials generally requires high optical powers to achieve appreciable nonlinear effects [28]. Direction-selective transmission devices based on the thermo-optic nonlinearity of silicon metasurfaces enable ultrathin designs and high transmission contrast at low input powers [21]. However, their reliance on precise beam alignment limits coupling efficiency and integration. In contrast, asymmetric microcavity structures introduce spatial asymmetry to modulate the intracavity nonlinear response. As a result, forward- and backward-propagating light experience different optical field distributions and nonlinear interaction processes, leading to pronounced direction-dependent transmission characteristics [29].

In this work, we report a simple method to achieve thermal-feedback-induced transmission symmetry breaking in an asymmetric fiber microcavity. Using polydimethylsiloxane (PDMS) and asymmetric microcavities, we systematically investigate how thermal feedback modulates cavity resonance and optical transmission. Due to the structural asymmetry of the cavity, forward and backward transmissions exhibit different coupling efficiencies, leading to distinct thermal feedback responses and ultimately resulting in transmission symmetry breaking. The results show that the device can achieve a transmission contrast exceeding 50 dB, demonstrating excellent asymmetric transmission performance.

2. System and model

Fig. 1 shows a schematic of the proposed asymmetric fiber Fabry-Pérot (FP) microcavity. The cavity is formed by two fiber end facets with unequal reflectivity, R_1 and R_2, respectively, and is filled with PDMS as the thermo-optic medium. Due to the different reflectivity at the two ends, the microcavity exhibits distinct external coupling loss rates κ_1 and κ_2, resulting in an asymmetric optical cavity structure. Therefore, the intracavity optical field distribution becomes asymmetric, which inducing nonuniform absorption of intracavity optical power in PDMS and generating a transient temperature imbalance between the two cavity regions. For a micrometer-scale PDMS-filled FP cavity, this thermal imbalance is expected to relax within a sub-second timescale due to thermal diffusion. The corresponding refractive index variation can be estimated as $\Delta n = (dn/dT)\Delta T$, where the thermo-optic coefficient of PDMS is approximately $dn/dT = -4.5\times10^{-4}$ K^{-1} [30]. Meanwhile, the thermal expansion-induced cavity-length variation follows $\Delta L = \alpha L \Delta T$, where the thermal expansion coefficient of PDMS is approximately $\alpha = 3\times10^{-4}$ K^{-1} [31]. Although the induced index and length changes are small, the high-finesse cavity significantly enhances their influence on the resonance condition, enabling strong thermo-optic nonlinear feedback.

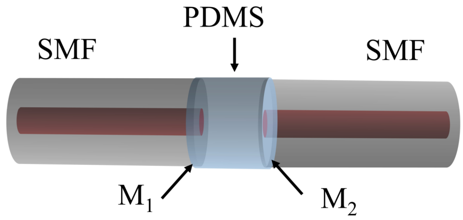

Fig. 1. Schematic of the system structure.

Therefore, forward and backward excitation produce different intracavity field distributions and absorption powers in PDMS, leading to distinct thermo-optic responses. The resulting temperature variations further modulate the refractive index and cavity length via thermo-optic and thermal expansion effects, inducing a temperature-dependent shift of the cavity resonance wavelength. This shift modifies the laser-cavity detuning, affecting the intracavity field buildup and giving rise to an asymmetric thermal feedback process governed by the unequal coupling strengths. Once the feedback exceeds a threshold, a pronounced thermo-optic nonlinear response emerges.

Starting from the Hamiltonian, the intracavity field dynamics can be obtained using the Heisenberg-Langevin formalism. By including all intrinsic and external loss channels, the evolution of the cavity field operator a is governed by

$$\dot{a} = \left(i\Delta - \frac{\kappa}{2}\right)a + \sqrt{\kappa_j}\, s_{\text{in}}, \tag{1}$$

where $\dot{a}$ represents the temporal evolution of the cavity field, and a denotes the complex amplitude of the intracavity optical field. $\Delta = \omega_L - \omega_c$ is the laser-cavity detuning, ω_L and ω_c are the angular frequencies of the input laser and the cavity resonance mode, respectively. The input field amplitude is represented by s_{in}, and j=1, 2 denotes excitation from the left or right port, respectively. The total cavity decay rate is given by $\kappa = \kappa_1 + \kappa_2 + \kappa_{\text{abs}} + \kappa_{\text{sca}}$, where κ_1 and κ_2 represent the mirror-induced loss rates associated with the two cavity facets, respectively. κ_{abs} accounts for material absorption in PDMS, and κ_{sca} represents scattering loss. According to the steady-state solution, the intracavity field amplitude is given by

$$a = \frac{\sqrt{\kappa_j}\, s_{\text{in}}}{\kappa/2 - i\Delta}. \tag{2}$$

Therefore, the intracavity photon number is given by

$$n_c = |a|^2 = \frac{\kappa_j |s_{\text{in}}|^2}{(\kappa/2)^2 + \Delta^2}. \tag{3}$$

Using the relation $P_{\text{in}} = \hbar\omega_L |s_{\text{in}}|^2$, P_{in} denotes the input optical power. The photon number can be expressed in terms of the input power as

$$n_c = \frac{\kappa_j P_{\text{in}}}{\hbar\omega_L\left[(\kappa/2)^2 + \Delta^2\right]}. \tag{4}$$

The intracavity optical energy is partially absorbed by the PDMS, which acts as the thermo-optic medium. The corresponding absorbed power can be expressed as $P_{\text{abs}} = \hbar\omega_c \kappa_{\text{abs}} n_c$. Substituting the intracavity photon number, the absorbed power becomes

$$P_{\text{abs}} = \frac{\omega_c}{\omega_L} \cdot \frac{\kappa_j \kappa_{\text{abs}}}{(\kappa/2)^2 + \Delta^2} P_{\text{in}}. \tag{5}$$

The absorbed optical power leads to a temperature rise in the PDMS, which can be described by the thermal balance equation

$$C_{\text{th}} \frac{dT}{dt} = P_{\text{abs}} - G_{\text{th}}(T - T_0), \tag{6}$$

where C_{th} is the thermal capacitance, G_{th} is the thermal conductance, and T_0 is the ambient temperature. Under steady-state conditions (dT/dt=0), the temperature increase is given by

$$\Delta T = \frac{P_{\text{abs}}}{G_{\text{th}}} == \frac{\kappa_j \kappa_{\text{abs}}}{G_{\text{th}}\left[(\kappa/2)^2 + \Delta^2\right]} P_{\text{in}}. \tag{7}$$

The temperature variation further modifies both the refractive index and the cavity length via the thermo-optic and thermal expansion effects, leading to a shift of the cavity resonance wavelength. This shift can be written as

$$\Delta\lambda_r = \beta\Delta T, \tag{8}$$

where $\beta \equiv \lambda_r\left(\frac{1}{n}\frac{dn}{dT}+\alpha\right)$. As a result, the cavity resonance becomes temperature-dependent, i.e., $\lambda_r \equiv \lambda_{r0}+\Delta\lambda_r$, which modifies the laser-cavity detuning as

$$\delta \equiv \lambda_L - \lambda_r = \delta_0 - \beta\Delta T, \tag{9}$$

where $\delta_0 = \lambda_L - \lambda_{r0}$ is the cold-cavity detuning. Substituting the steady-state temperature rise into the above expression yields a self-consistent relation for the detuning

$$\delta = \delta_0 - \frac{\beta\kappa_j\kappa_{\text{abs}}}{G_{\text{th}}\left[(\kappa/2)^2+\delta^2\right]}P_{\text{in}}. \tag{10}$$

This equation indicates that the cavity detuning depends nonlinearly on the intracavity field through the thermal feedback effect, forming a closed-loop optothermal interaction. Due to the asymmetric coupling rates $\kappa_1 \neq \kappa_2$, the absorbed power-and consequently the temperature rise-differs for forward and backward excitation. As a result, the steady-state solutions of the above self-consistent equation become direction-dependent, i.e., $\delta_F \neq \delta_B$, leading to asymmetric intracavity fields and ultimately giving rise to thermal-induced asymmetric transmission in the asymmetric FP microcavity. The cavity transmission can be expressed as

$$T_j = \frac{\kappa_1\kappa_2}{(\kappa_0/2)^2+\delta_j^2}, \quad (j = F, B), \tag{11}$$

where δ_j denotes the thermally modified detuning for each propagation direction. Although the transmission formula retains a symmetric analytical form, the implicit dependence of δ_j on the direction-dependent thermal response results in $T_F \neq T_B$, thereby giving rise to thermal-feedback-mediated transmission symmetry breaking in the asymmetric FP microcavity.

Before investigating transmission symmetry breaking in the asymmetric FP cavity, we first analyze the intrinsic thermo-optic nonlinear response of a PDMS-filled symmetric FP cavity. In this case, the two cavity mirrors have identical reflectivities ($R_1 = R_2 = 0.9999$), and the cavity is used only to characterize the thermal feedback effect induced by PDMS. This configuration does not introduce directional asymmetry but provides a fundamental understanding of the thermal nonlinear behavior.

Fig. 2 shows the thermo-optic nonlinear dynamic transmission response of the PDMS-filled symmetric FP microcavity. The red curve in the upper panel denotes a linear bidirectional wavelength sweep of the input signal, which periodically modulates the cavity detuning. Due to the large thermo-optic response of PDMS, the absorbed optical power induces temperature variations that modify the effective refractive index and cavity length, resulting in a dynamic shift of the cavity resonance. During the downward wavelength scan from 1550.4 nm to 1549.5 nm, the transmission response exhibits an apparent broadening due to thermally induced nonlinear feedback. In contrast, during the upward wavelength scan from 1549.5 nm to 1550.4 nm, the resonance response becomes narrower. This opposite spectral evolution indicates a pronounced hysteresis behavior during wavelength scanning. The observed asymmetry originates from the nonlinear interaction between optical absorption and thermally induced resonance shifts, while the finite thermal response time leads to delayed temperature evolution relative to the optical field dynamics.

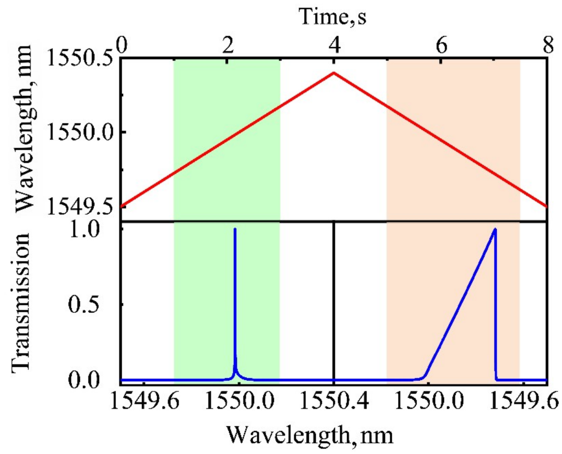

Fig. 2. Temporal evolution of the input wavelength and corresponding transmission spectra of the FP microcavity. The upper panel shows the time-dependent wavelength tuning, while the lower panel presents the corresponding transmission response under wavelength up-sweep (green region) and down-sweep (orange region) conditions. Relevant parameters: $R_1 = R_2 = 0.9999$, $P_{in} = 1$ mW, the index is $n = 1.41$, the cavity length is 100 µm.

3. Result and discussion

Building on the observed scan-direction-dependent broadening under the laser downward sweep, we exploit this effect as a mechanism for asymmetric transmission design in the asymmetric FP microcavity. Fig. 3 indicates the transmission characteristics of the asymmetric FP microcavity under a downward wavelength sweep from 1550.4 nm to 1549.0 nm. The reflectivity of mirror M_1 is fixed at $R_1 = 0.999$, while the reflectivity of mirror M_2 is gradually increased to investigate its influence on the thermo-optic asymmetric transmission. Figs. 2a–d present the transmitted power for light incident from opposite

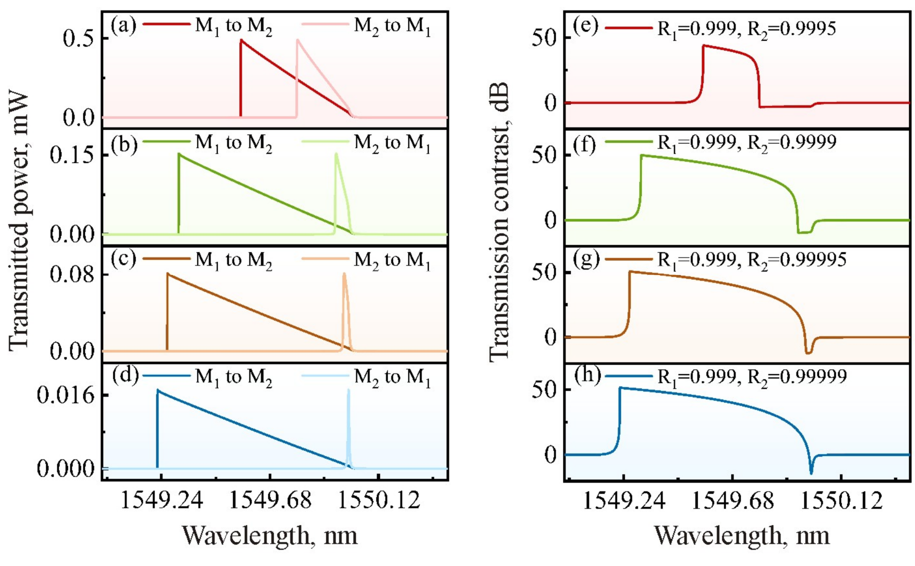

Fig. 3. Simulated transmission characteristics of the asymmetric FP microcavity under a downward wavelength sweep from 1550.4 nm to 1549.0 nm. (a)–(d) Transmitted power for light incident from M_1 to M_2 and from M_2 to M_1 with a fixed reflectivity $R_1 = 0.999$ and different values of R_2: (a) 0.9995, (b) 0.9999, (c) 0.99995, and (d) 0.99999. (e)–(h) Corresponding transmission contrast for the same reflectivity configurations. Other parameters: $P_{in} = 1$ mW, the index is $n = 1.41$, the cavity length is 100 µm.

directions ($M_1 \rightarrow M_2$ and $M_2 \rightarrow M_1$) with different values of R_2. When the cavity asymmetry is weak (R_2 = 0.9995), the transmission difference between the two propagation directions is relatively limited. As R_2 increases from 0.9995 to 0.99999, the transmission for the $M_1 \rightarrow M_2$ direction exhibits an increasingly broadened nonlinear response, whereas the transmission in the opposite direction remains highly localized near the resonance wavelength. Consequently, the transmission asymmetry is continuously enhanced with increasing cavity reflectivity contrast.

Figs. 3e–h demonstrate the corresponding transmission contrast. The maximum transmission contrast increases with increasing R_2, reaching nearly 50 dB when R_2 = 0.99999. Meanwhile, the high-contrast wavelength range is also broadened, indicating that a stronger cavity asymmetry enhances the thermo-optic feedback and enlarges the operating window for direction-selective transmission. The improvement originates from the stronger intracavity field localization introduced by the asymmetric cavity. A higher reflectivity at M_2 increases the optical intensity and thermal accumulation inside the cavity, thereby strengthening the thermo-optic nonlinear feedback. As a result, the resonance shift becomes more pronounced during the wavelength sweep, leading to enhanced transmission asymmetry and a higher transmission contrast.

Fig. 4 displays the transmission characteristics of the asymmetric FP microcavity under a downward wavelength sweep from 1550.4 nm to 1549.0 nm for different input powers. The cavity reflectivity is fixed at R_1 = 0.999 and R_2 = 0.99999. As shown in Figs. 4a-d, the transmitted power is plotted for light propagating in the $M_1 \rightarrow M_2$ and $M_2 \rightarrow M_1$ directions. At a low input power of 1 μW, the transmission spectra for the two propagation directions almost completely overlap. As the input power increases, the transmission in the $M_1 \rightarrow M_2$ direction gradually evolves into a broadened nonlinear response, whereas the transmission in the opposite direction remains nearly unchanged. Consequently, the transmission asymmetry becomes increasingly pronounced with increasing input power.

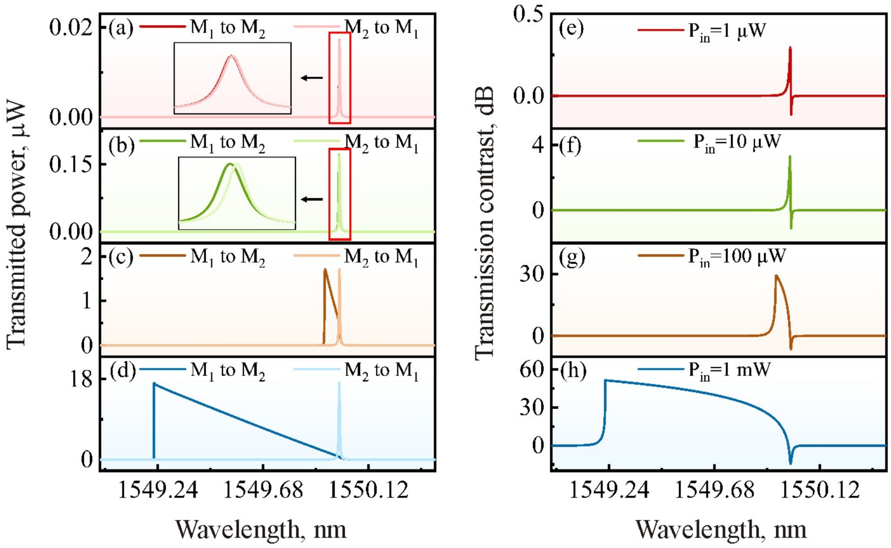

Fig. 4. Simulated transmission characteristics of the asymmetric FP microcavity under a downward wavelength sweep from 1550.4 nm to 1549.0 nm for different input powers. (a)–(d) transmitted power for light incident from M_1 to M_2 and from M_2 to M_1 with input powers of: (a) 1 μW, (b) 10 μW, (c) 100 μW, and (d) 1 mW. (e–h) corresponding transmission contrast for different input powers. Other parameters: R_1 =0.999, R_2 = 0.99999, the index is n = 1.41, and the cavity length is 100 μm.

The corresponding transmission contrast is illustrated in Figs. 4e–h. The transmission contrast increases monotonically as input power increases and reaches nearly 50 dB at 1 mW. In addition, the wavelength range exhibiting high transmission contrast becomes significantly broader at higher input powers, indicating an enlarged operating window for direction-selective transmission. The enhanced transmission asymmetry originates from the stronger thermo-optic nonlinear feedback at higher optical powers. As the intracavity optical intensity increases, thermal accumulation becomes more significant, leading to a larger resonance shift during wavelength sweeping. Consequently, the transmission difference between the two propagation directions is substantially enhanced, resulting in a higher transmission contrast.

Fig. 5 clearly depicts the transmission behavior of the thermo-optic asymmetric FP microcavity at different cavity lengths during a descending wavelength sweep from 1550.4 nm to 1549.0 nm. The mirror reflectivities are fixed at R_1 = 0.999 and R_2 = 0.99999, and the input optical power is fixed at 1 μW. The cavity length L is systematically varied to investigate its influence on thermo-optic asymmetric transmission. Figs. 5a-e present the transmitted power for light incident from opposite directions at five cavity lengths: L = 20 μm, 40 μm, 60 μm, 80 μm, and 100 μm. When the cavity length is short (L = 20 μm), the nonlinear transmission spectrum in the $M_1 \rightarrow M_2$ direction shows a narrow power peak with a limited wavelength range of nonlinear response, while the transmission in the opposite $M_2 \rightarrow M_1$ direction remains highly localized near the resonant wavelength. As L increases from 20 μm to 100 μm, the transmission curve for the $M_1 \rightarrow M_2$ direction exhibits a broadened nonlinear tail and increased peak transmitted power, whereas the counter-propagating transmission remains tightly confined around resonance. Consequently, the transmission asymmetry between the two opposite propagation directions continuously increases with cavity length.

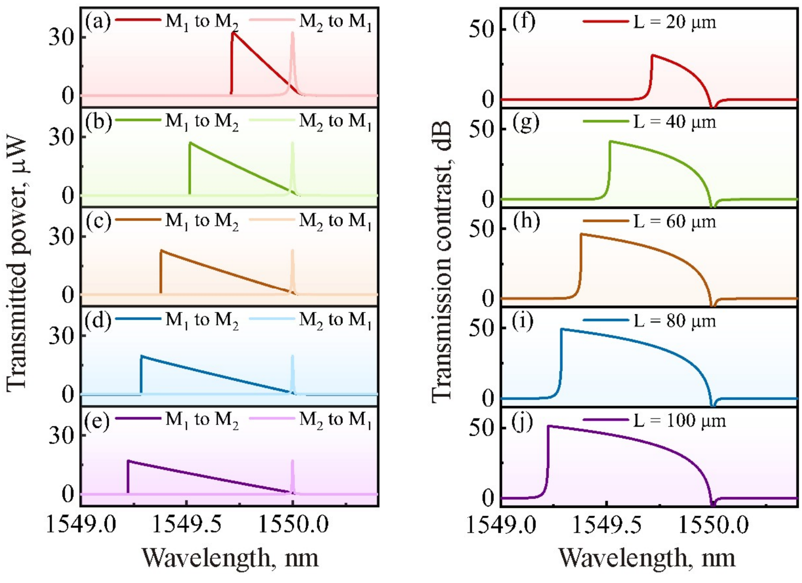

Fig. 5. Simulated transmission characteristics of the asymmetric FP microcavity under a downward wavelength sweep from 1550.4 nm to 1549.0 nm for different cavity lengths. (a)–(d) transmitted power for light incident from M_1 to M_2 and from M_2 to M_1 with cavity length of: (a) L = 20 μm, (b) L = 40 μm, (c) 60 μm, (d) L = 80 μm, and (e) L = 100 μm. (f) - (j) corresponding transmission contrast for the different cavity lengths. Other parameters: R_1 = 0.999, R_2 = 0.99999, P_{in} = 1 mW the index is n =1.41.

The corresponding transmission-contrast curves at each cavity length are shown in Figs. 5f-j. The maximum transmission contrast increases monotonically with cavity length. The wavelength range with high transmission contrast also broadens, indicating that a longer resonant cavity strengthens intracavity thermo-optic feedback and enlarges the operating wavelength window for direction-selective transmission. The increased cavity length enhances light-matter interaction, boosting circulating intensity and thermo-optic refractive-index modulation. This reinforces nonlinear thermal feedback, producing a larger resonance shift during the downward wavelength sweep and greater spectral separation between bidirectional responses, thereby improving transmission asymmetry and peak contrast over a wider wavelength range.

The proposed transmission symmetry-breaking mechanism is induced by thermo-optic feedback. Therefore, its practical operation speed is governed by the thermal relaxation dynamics of the cavity. The transient temperature evolution can be described by the thermal balance equation given in Eq. (6). The corresponding thermal relaxation time is given by $\tau_{\mathrm{th}} = C_{\mathrm{th}} / G_{\mathrm{th}}$, which characterizes the response time of the thermo-optic feedback process. Accordingly, the thermal modulation bandwidth can be approximately estimated as $f_{\mathrm{th}} \approx 1/(2\pi\tau_{\mathrm{th}})$. Compared with the intrinsic photon lifetime of the FP cavity, the thermal relaxation process is much slower and therefore dominates the overall response speed of the device. As a result, the proposed scheme is more suitable for compact and reconfigurable photonic applications requiring controllable asymmetric transmission, such as nonlinear optical signal processing and integrated photonic control, rather than ultrafast optical switching.

4. Implementation

The proposed transmission symmetry-breaking scheme can be experimentally implemented using an asymmetric fiber FP microcavity filled with a thermo-optic nonlinear medium. In our design, PDMS is selected as the intracavity medium due to its large thermo-optic coefficient and high optical transparency in the near-infrared wavelength region. Such properties enable efficient modulation of the cavity resonance through absorption-induced temperature variations.

The asymmetric FP cavity can be realized by coating the two fiber end faces with dielectric films of different reflectivity, thereby introducing asymmetric mirror reflectivity. Such fiber-end-face coating techniques have been widely employed to fabricate high-finesse fiber FP microcavities and have been experimentally demonstrated in previous studies [32]. Due to the asymmetric coupling rates at the two cavity mirrors, forward- and backward-propagating light experience different intracavity power distributions, resulting in different absorption-induced thermal responses.

In practice, a tunable laser around 1550 nm can be coupled into the asymmetric FP cavity through either side of the fiber device, and the transmitted optical powers in the two propagation directions can be recorded using a photodetector. The transmission symmetry breaking can then be characterized by comparing the forward and backward transmission spectra. Similar fiber-based FP microcavities with high-reflectivity dielectric mirrors and liquid/polymer-filled microcavities have been experimentally demonstrated for high-sensitivity optical sensing and nonlinear optical modulation [33]. Therefore, the proposed thermo-optic transmission symmetry-breaking mechanism can be realized using existing fiber microcavity fabrication and optical measurement techniques.

5. Conclusions

In summary, we have demonstrated an asymmetric FP microcavity with a transmission contrast exceeding 50 dB. This pronounced transmission asymmetry arises from the interplay between cavity asymmetry and thermo-optic nonlinear feedback. The proposed scheme is experimentally feasible owing to its simple fiber-compatible architecture and does not rely on magneto-optic materials or external bias fields. Moreover, the broadband enhancement achieved via cavity-length optimization suggests potential scalability of the proposed scheme for integrated photonic implementations. Overall, this work establishes a simple yet effective platform for controllable transmission asymmetry in microcavities, which may find applications in direction-dependent optical signal processing and on-chip asymmetric photonic devices.

Funding. This research received no external funding.

Data availability. The data can be obtained from the authors upon request.

Conflict of interest. The authors declare no conflict of interest. The authors declare that they have no known competing financial interests or personal relationships that could have influenced the work reported in this paper.

Author's contributions. M.S. conceived the idea, developed the theoretical model, performed the theoretical calculations, prepared the figures, and wrote the manuscript. G.S. contributed to verifying the theoretical results, performing numerical analyses, and discussing the results. M.S. supervised the project and finalized the manuscript.

References

1. Iwamura, H., Hayashi, S., & Iwasaki, H. (1978). A compact optical isolator using a $Y_3Fe_5O_{12}$ crystal for near infra-red radiation. *Optical and Quantum Electronics, 10*, 393–398.
2. Gauthier, D. J., Narum, P., & Boyd, R. W. (1986). Simple, compact, high-performance permanent-magnet Faraday isolator. *Optics Letters, 11*(10), 623–625.
3. Dötsch, H., Bahlmann, N., Zhuromskyy, O., Hammer, M., Wilkens, L., Gerhardt, R., Hertel, P., & Popkov, A. F. (2005). Applications of magneto-optical waveguides in integrated optics: Review. *Journal of the Optical Society of America B, 22*(1), 240–253.
4. Bi, L., Hu, J., Jiang, P., Kim, D. H., Dionne, G. F., Kimerling, L. C., & Ross, C. A. (2011). On-chip optical isolation in monolithically integrated non-reciprocal optical resonators. *Nature Photonics, 5*, 758–762.
5. Ren, S. Y., Yan, W., Feng, L. T., Chen, Y., Wu, Y. K., Qi, X. Z., Liu, X. J., Cheng, Y. J., Xu, B. Y., Deng, L. J., Guo, G. C., Bi, L., & Ren, X. F. (2022). Single-photon nonreciprocity with an integrated magneto-optical isolator. *Laser & Photonics Reviews, 16*(5), 2100595.
6. Peng, P., Thapa, G., Zhou, J., & Talbayev, D. (2023). Emergent optical nonreciprocity and chirality-controlled magneto-optical resonance in a hybrid magneto-chiral metamaterial. *Optica, 10*(2), 155–161.
7. Lira, H., Yu, Z., Fan, S., & Lipson, M. (2012). Electrically driven nonreciprocity induced by interband photonic transition on a silicon chip. *Physical Review Letters, 109*, 033901.
8. Yu, Z., & Fan, S. (2009). Complete optical isolation created by indirect interband photonic transitions. *Nature Photonics, 3*, 91–94.
9. Tian, H., Liu, J., Siddharth, A., Wang, R. N., Blesin, T., He, J., Kippenberg, T. J., & Bhave, S. A. (2021). Magnetic-free silicon nitride integrated optical isolator. *Nature Photonics, 15*, 828.
10. Guo, X., Ding, Y., Duan, Y., & Ni, X. (2019). Nonreciprocal metasurface with space-time phase modulation. *Light: Science & Applications, 8*, 123.
11. Xu, L., Huang, J., & Ouyang, X. (2021). Tunable thermal wave nonreciprocity by spatiotemporal modulation. *Physical Review E, 103*, 032128.
12. Wu, J., & Yousefzadeh, B. (2024). Nonreciprocal energy transmission in short discrete systems with strong spatiotemporal modulations. *Journal of the Acoustical Society of America, 155*(3), A121.
13. Wang, D. W., Zhou, H. T., Guo, M. J., Zhang, J. X., Evers, J., & Zhu, S. Y. (2013). Optical diode made from a moving photonic crystal. *Physical Review Letters, 110*, 093901.

14. Horsley, S. A. R., Wu, J. H., Artoni, M., & La Rocca, G. C. (2013). Optical nonreciprocity of cold atom Bragg mirrors in motion. *Physical Review Letters, 110*, 223602.
15. Ramezani, H., Jha, P. K., Wang, Y., & Zhang, X. (2018). Nonreciprocal localization of photons. *Physical Review Letters, 120*, 043901.
16. Manipatruni, S., Robinson, J. T., & Lipson, M. (2009). Optical nonreciprocity in optomechanical structures. *Physical Review Letters, 102*, 213903.
17. Shen, Z., Zhang, Y. L., Chen, Y., Zou, C. L., Xiao, Y. F., Zou, X. B., Sun, F. W., Guo, G. C., & Dong, C. H. (2016). Experimental realization of optomechanically induced non-reciprocity. *Nature Photonics, 10*, 657–661.
18. Xu, X., Zhao, Y., Wang, H., Jing, H., & Chen, A. (2020). Quantum nonreciprocity in quadratic optomechanics. *Photonics Research, 8*(2), 143–150.
19. Yang, K. Y., Skarda, J., Cotrufo, M., Dutt, A., Ahn, G. H., Sawaby, M., Vercruysse, D., Arbabian, A., Fan, S., Alù, A., & Vučković, J. (2020). Inverse-designed non-reciprocal pulse router for chip-based LiDAR. *Nature Photonics, 14*, 369–374.
20. Sounas, D. L., Soric, J., & Alù, A. (2018). Broadband passive isolators based on coupled nonlinear resonances. *Nature Electronics, 1*, 113–119.
21. Cotrufo, M., Cordaro, A., Sounas, D. L., Polman, A., & Alù, A. (2024). Passive bias-free nonreciprocal metasurfaces based on thermally nonlinear quasi-bound states in the continuum. *Nature Photonics, 18*, 81.
22. Del Bino, L., Silver, J. M., Woodley, M. T. M., Stebbings, S. L., Zhao, X., & Del'Haye, P. (2018). Microresonator isolators and circulators based on the intrinsic nonreciprocity of the Kerr effect. *Optica, 5*(3), 279–282.
23. Sounas, D. L., & Alù, A. (2018). Fundamental bounds on the operation of Fano nonlinear isolators. *Physical Review B, 97*, 115431.
24. Yang, S., Liu, M., Zhao, C., Fan, S., & Qiu, C. W. (2024). Nonreciprocal thermal photonics. *Nature Photonics, 18*, 412.
25. Li, B., Özdemir, S. K., Xu, X. W., Zhang, L., Kuang, L. M., & Jing, H. (2021). Nonreciprocal optical solitons in a spinning Kerr resonator. *Physical Review A, 103*, 053522.
26. Yu, Z. F., Yan, P. F., Wang, Y., Xu, H. P., Zhang, A. X., & Xue, J. K. (2025). Kerr nonlinearity regulated nonreciprocal amplification in cavity magnon polaritons. *Optics Letters, 50*(18), 5885–5888.
27. Ren, L. H., Xu, X. B., Zhu, S., Shi, L., & Zhang, X. L. (2020). Experimental realization of on-chip nonreciprocal transmission by using the mechanical Kerr effect. *ACS Photonics, 7*(11), 2995–3002.
28. Shi, Y., Yu, Z., & Fan, S. (2015). Limitations of nonlinear optical isolators due to dynamic reciprocity. *Nature Photonics, 9*, 388.
29. Yang, P. F., Xia, X. W., He, H., Li, S. K., Han, X., Zhang, P., Li, G., Zhang, P. F., Xu, J. P., Yang, Y. P., & Zhang, T. C. (2019). Realization of nonlinear optical nonreciprocity on a few-photon level based on atoms strongly coupled to an asymmetric cavity. *Physical Review Letters, 123*, 233604.
30. Markos, C., Vlachos, K., & Kakarantzas, G. (2010). Bending loss and thermo-optic effect of a hybrid PDMS/silica photonic crystal fiber. *Optics Express, 18*(23), 24344–24351.
31. Veysset, D., Ling, T., Zhu, Y., Pandiyan, V. P., Sabesan, R., & Palanker, D. (2022). Interferometric imaging of thermal expansion for temperature control in retinal laser therapy. *Biomedical Optics Express, 13*(2), 728–743.
32. Ott, K., Garcia, S., Kohlhaas, R., Schüppert, K., Rosenbusch, P., Long, R., & Reichel, J. (2016). Millimeter-long fiber Fabry–Perot cavities. *Optics Express, 24*(9), 9839–9853.
33. Yan, Y., Xiao, X., Nie, Q., Wang, Z., Chen, Y., Wu, J., Zhou, N., Zhou, R., Yang, S., & Ren, W. (2024). Nanoliter-scale light–matter interaction in a fiber-tip cavity enables sensitive photothermal gas detection. *Laser & Photonics Reviews, 18*(12), 2400907.

She, M., Shi, G. (2026). Thermal-Feedback-Induced Transmission Symmetry Breaking in an Asymmetric Microcavity. *Ukrainian Journal of Physical Optics*, *27*(4), 04077 – 04087.
doi: 0.3116/16091833/Ukr.J.Phys.Opt.2026.04077

Анотація. *Порушення симетрії пропускання є важливим для реалізації напрямково-селективного транспорту світла в інтегрованій фотоніці, тоді як наявні підходи зазвичай спираються на магнітооптичні матеріали, часову модуляцію або сильні оптичні нелінійності. Ми теоретично досліджуємо порушення симетрії пропускання, індуковане тепловим зворотним зв'язком, в асиметричному мікрорезонаторі Фабрі-Перо, заповненому полідиметилсилоксаном. Через неоднакові відбивні здатності дзеркал зустрічно поширювані оптичні поля мають різну ефективність зв'язку та поглинання, що призводить до різних термічно індукованих резонансних зміщень і характеристик* *пропускання. Числові результати показують, що запропонована немагнітна структура може досягти контрасту пропускання, що перевищує 50 дБ. Запропонований механізм забезпечує простий підхід до реалізації компактних інтегрованих фотонних пристроїв з напрямково-селективним пропусканням.*

Ключові слова: *термооптична нелінійність, асиметричний мікрорезонатор Фабрі-Перо, порушення симетрії пропускання, волоконно-інтегровані пристрої*